

Charge density wave states in phase-engineered monolayer VTe2

Zhi-Li Zhu(朱知力)1, Zhong-Liu Liu(刘中流)1, Xu Wu(武旭)2,1, Xuan-Yi Li(李轩熠)1, Jin-An Shi(时金安)1, Chen Liu(刘晨)3, Guo-Jian Qian(钱国健)1, Qi Zheng(郑琦)1, Li Huang(黄立)1, Xiao Lin(林晓)1, Jia-Ou Wang(王嘉欧)3, Hui Chen(陈辉)1, Wu Zhou(周武)1, Jia-Tao Sun(孙家涛)2,1, Ye-Liang Wang(王业亮)2,1,†, and Hong-Jun Gao(高鸿钧)1,‡

Citation: Chin. Phys. B, 2022, 31 (7): 077101 DOI: 10.1088/1674-1056/ /ac6739
Journal homepage: http://cpb.iphy.ac.cn; http://iopscience.iop.org/cpb

What follows is a list of articles you may be interested in

Effect of strain on charge density wave order in α-U

Liuhua Xie(谢刘桦), Hongkuan Yuan(袁宏宽), and Ruizhi Qiu(邱睿智)
Chin. Phys. B, 2022, 31 (**6**): 067103. DOI: 10.1088/1674-1056/ac4f4d

Tri-hexagonal charge order in kagome metal CsV_3Sb_5 revealed by ^{121}Sb nuclear quadrupole resonance

Chao Mu(牟超), Qiangwei Yin(殷蔷薇), Zhijun Tu(涂志俊), Chunsheng Gong(龚春生), Ping Zheng(郑萍), Hechang Lei(雷和畅), Zheng Li(李政), and Jianlin Luo(雒建林)
Chin. Phys. B, 2022, 31 (**1**): 017105. DOI: 10.1088/1674-1056/ac422c

Direct observation of melted Mott state evidenced from Raman scattering in 1T-TaS_2 single crystal

Qing Hu(胡庆), Cong Yin(尹聪), Leilei Zhang(张雷雷), Li Lei(雷力), Zhengshang Wang(王正上), Zhiyu Chen(陈志禹), Jun Tang(唐军), Ran Ang(昂然)
Chin. Phys. B, 2018, 27 (**1**): 017104. DOI: 10.1088/1674-1056/27/1/017104

High sensitivity refractive index gas sensing enhanced by surface plasmon resonance with nano-cavity antenna array

Zhao Hua-Jun
Chin. Phys. B, 2012, 21 (**8**): 087104. DOI: 10.1088/1674-1056/21/8/087104

RAPID COMMUNICATION

Charge density wave states in phase-engineered monolayer VTe_2

Zhi-Li Zhu(朱知力)[1], Zhong-Liu Liu(刘中流)[1], Xu Wu(武旭)[2,1], Xuan-Yi Li(李轩熠)[1], Jin-An Shi(时金安)[1], Chen Liu(刘晨)[3], Guo-Jian Qian(钱国健)[1], Qi Zheng(郑琦)[1], Li Huang(黄立)[1], Xiao Lin(林晓)[1], Jia-Ou Wang(王嘉欧)[3], Hui Chen(陈辉)[1], Wu Zhou(周武)[1], Jia-Tao Sun(孙家涛)[2,1], Ye-Liang Wang(王业亮)[2,1,†], and Hong-Jun Gao(高鸿钧)[1,‡]

[1] *Institute of Physics and University of Chinese Academy of Sciences, Chinese Academy of Sciences, Beijing* 100190, *China*
[2] *MIIT Key Laboratory for Low-Dimensional Quantum Structure and Devices, School of Integrated Circuits and Electronics, Beijing Institute of Technology, Beijing* 100081, *China*
[3] *Institute of High Energy Physics, Chinese Academy of Sciences, Beijing* 100084, *China*

(Received 7 March 2022; revised manuscript received 11 April 2022; accepted manuscript online 14 April 2022)

Charge density wave (CDW) strongly affects the electronic properties of two-dimensional (2D) materials and can be tuned by phase engineering. Among 2D transitional metal dichalcogenides (TMDs), VTe_2 was predicted to require small energy for its phase transition and shows unexpected CDW states in its T-phase. However, the CDW state of H-VTe_2 has been barely reported. Here, we investigate the CDW states in monolayer (ML) H-VTe_2, induced by phase-engineering from T-phase VTe_2. The phase transition between T- and H-VTe_2 is revealed with x-ray photoelectron spectroscopy (XPS) and scanning transmission electron microscopy (STEM) measurements. For H-VTe_2, scanning tunneling microscope (STM) and low-energy electron diffraction (LEED) results show a robust $2\sqrt{3}\times 2\sqrt{3}$ CDW superlattice with a transition temperature above 450 K. Our findings provide a promising way for manipulating the CDWs in 2D materials and show great potential in its application of nanoelectronics.

Keywords: charge density wave, H-VTe_2, phase engineering, transitional metal dichalcogenides

PACS: 71.45.Lr, 64.60.–i, 68.65.–k **DOI:** 10.1088/1674-1056/ac6739

1. Introduction

As a collective phenomenon of great interest in condensed matter physics, charge density wave (CDW)[1] is discovered in many transitional metal dichalcogenides (TMDs).[2] In this group of two-dimensional (2D) materials with diverse components and unique properties, the CDW transition not only reflects diverse spatial and electronic structure with complicated origins,[3–6] but also exhibit great potential for applications.[7–12] For the required manipulation, phase engineering[13] is an effective method to modify both the structural and electronic properties of TMDs,[14,15] including CDWs.[14,16] Such manipulation usually requires energy to overcome the barrier between different phases.[15,17,18] Thus, phase engineering is more effective on a TMD material with a smaller formation energy difference between phases.

Among TMDs, vanadium dichalcogenides (VX_2, X = S, Se, Te) are drawing tremendous attention recently and have been reported with several unexpected CDW states and electronic properties.[19–27] According to the previous calculation results,[28–31] T and H-phase VX_2 share very similar forming energy, especially for VTe_2, meaning a high possibility for phase engineering. The experimental reports of CDW in VTe_2 are focused on its T-phase, which is the stable phase in its bulk. However, the report on CDW states of H-VTe_2 is still rare, in spite of the intense theoretical calculations.[30–35]

In this study, we report the phase-engineering of monolayer (ML) VTe_2 from T-phase to H-phase and its induced robust CDW states. Epitaxial T-phase VTe_2 is transformed into H-phase with an annealing process, which is confirmed by XPS and cross-section STEM results. The STM and LEED results reveal that the ML T-VTe_2 has a 4×4 CDW superlattice at low temperature, while the ML H-VTe_2 is found to exhibit a robust $2\sqrt{3}\times 2\sqrt{3}$ CDW superlattice with a transition temperature above 450 K. Thus, phase engineering not only induces robust CDW states in ML VTe_2 with applications in optoelectronics[7] and electronics,[9,10] but also provide a promising approach to manipulating the CDW behavior in 2D TMDs and exploring its nature.

2. Experimental section

2.1. Sample preparation

The sample of monolayer T-VTe_2 on epitaxial graphene on silicon carbide (Gr/SiC) was fabricated in an ultrahigh vacuum (UHV) chamber with the base pressure of 4×10^{-10} mbar (1 bar = 10^5 Pa), which was equipped with standard MBE facilities. The Gr/SiC substrate was prepared by annealing the doped SiC crystalline substrate (TankeBlue) at 1500 K

†Corresponding author. E-mail: yeliang.wang@bit.edu.cn
‡Corresponding author. E-mail: hjgao@iphy.ac.cn

© 2022 Chinese Physical Society and IOP Publishing Ltd

for 40 minutes after degassing at 900 K for 1 hour. Vanadium (ESPI Metals, 99.999%) atoms and tellurium (Sigma, 99.999%) atoms were deposited on Gr/SiC substrate from an electron-beam evaporator and a Knudsen cell, with the substrate temperature of 510 K. The grown process was under Te-rich condition, aiming to guarantee that enough Te atoms react with V atoms. And the growth rate of T-VTe_2 on Gr/SiC is about one layer per hour. Partial transformed H-VTe_2 was obtained by annealing T-VTe_2 at 530 K for 40 minutes in an ultrahigh vacuum condition.

2.2. XPS measurements

The *in-situ* x-ray photoelectron spectroscopy measurements of as-grown and annealed samples were performed in the Beijing Synchrotron Radiation Facility (BSRF). Synchrotron radiation light, which was monochromated by four high-resolution gratings and controlled by a hemispherical energy analyzer, has photon energy from 10 eV to 1100 eV.

2.3. STEM measurements

Before STEM measurements, we firstly deposited 10-nm C_{60} and 50-nm Sb on as-grown T-VTe_2 and partial transformed H-VTe_2 on Gr/SiC, aiming to protect the sample from oxidation and damage. Then the samples were sliced along SiC($11\bar{2}0$) face by a focused ion beam (FIB) and were further thinned to around 40-nm thickness using low-energy ion milling. And the cross-section high-angle annular dark-field scanning transmission electron microscopy (HAADF-STEM) images were obtained with an aberration-corrected STEM operated at 100 kV.

2.4. STM and LEED measurements

All the *in-situ* STM measurements were carried out in ultrahigh vacuum condition, with a base pressure under 4×10^{-10} mbar, in the constant-current mode, at room temperature (RT) (300 K) and 4.5 K. The *in-situ* LEED characterizations were carried out by an Omicron LEED system, with the base pressure under 4×10^{-10} mbar. The results were obtained with the electron energy of 40 eV.

2.5. ARPES measurements

ARPES measurements were performed at the photoelectron spectroscopy end station of the Beijing Synchrotron Radiation Facility 4B9B beamline. The experiments used He I ($h\nu = 21.2$ eV) resonance lines and a VG SCIENTA R4000 analyzer with the instrument energy resolution was better than 30 meV, and the angular resolution was 0.3°. All the data were recorded in UHV (better than 3×10^{-10} mbar, 1 bar $= 10^5$ Pa) at room temperature.

2.6. DFT calculations

The first-principles calculations for the geometry optimization and electronic structures of VTe_2 monolayers are performed by using the Vienna *ab initio* simulation package (VASP).[36] The projector augmented wave (PAW)[37] pseudopotentials and the generalized gradient approximation (GGA) exchange–correlation functionals proposed by Perdew, Burke, and Ernzerhof (PBE)[38] are used. The $11 \times 11 \times 1$ *k*-point grid is used in geometry optimization with a free energy tolerance of 10^{-5} eV and a force tolerance of 0.01 eV/Å. Spin-orbit coupling is included when calculating the band structures. A vacuum of 25 Å is adopted to avoid the vertical direction interactions between periodic layers.

2.7. Results and discussion

High-quality monolayer T-VTe_2 was fabricated on Gr/SiC substrate in an ultrahigh vacuum chamber through co-evaporating of V and Te atoms with the substrate temperature of 510 K (see Sample preparation). And with further annealing of the as-grown sample at 530 K for 40 min, T-VTe_2 will partially transform to H-VTe_2, as shown in Fig. 1(a). The XPS characterization results of as-grown and annealed samples in Fig. 1(b) show that the binding energy of Te 3d5/2 and 3d3/2 for the as-grown sample is 572.0 eV and 582.4 eV, agreeing with previous work about T-VTe_2.[27] While, there is another set of peaks at 572.3 eV and 582.7 eV for annealed sample, which shows an energy shift of 0.3 eV to the T-VTe_2 peaks. This extra set of peaks implies an emergent new phase of VTe_2.

To characterize the atomic structure of the emergent phase, we performed cross-section STEM measurements on the T-VTe_2 and T/H-VTe_2 samples. As shown in Figs. 2(a) and 2(d), the T and H phase VTe_2 can be clearly distinguished from the side view of the atomic model. In the STEM results shown in Figs. 2(b) and 2(e), the cross-section image of the VTe_2, corresponding to the side view atomic model, reveals the structure of T and H-VTe_2 unambiguously. From the line profiles shown in Figs. 2(c) and 2(f), we can read the size of the marked unit cell is 0.31 nm and 0.32 nm for T and H-VTe_2, respectively. Then, we can calculate that the lattice constant of T and H-VTe_2 is 0.35 nm and 0.36 nm, respectively. Thus, we prove that the phase-engineering of monolayer VTe_2 can be performed from T to H-phase through a transition process by annealing, demonstrated by the combination of XPS and cross-section STEM results.

To characterize the VTe_2 sample in detail, we performed the room temperature (RT) STM and LEED measurements on the as-prepared and annealed VTe_2 sample. Figure 3(a) shows the STM image of the monolayer T-VTe_2 islands in the as-prepared VTe_2 sample, which are clean and uniform, indicating the high quality of the fabricated film. As shown in Fig. 3(b), the apparent height of the T-VTe_2 island is 0.98 nm. The LEED pattern reveals the six-fold T-VTe_2 lattice shown

in Fig. 3(c). For the annealed sample, besides the T-VTe_2 islands, there are islands with irregular boundaries and 0.95-nm apparent height, which are the H-VTe_2 islands, as shown in Figs. 3(d) and 3(e). These H-VTe_2 islands are dominated in the annealed sample. Thus, in the LEED pattern shown in Fig. 3(f), we can see the spots of $2\sqrt{3}\times 2\sqrt{3}$ superlattice and its secondary diffraction spots appeared, which is absent in that of the as-prepared T-VTe_2 sample.

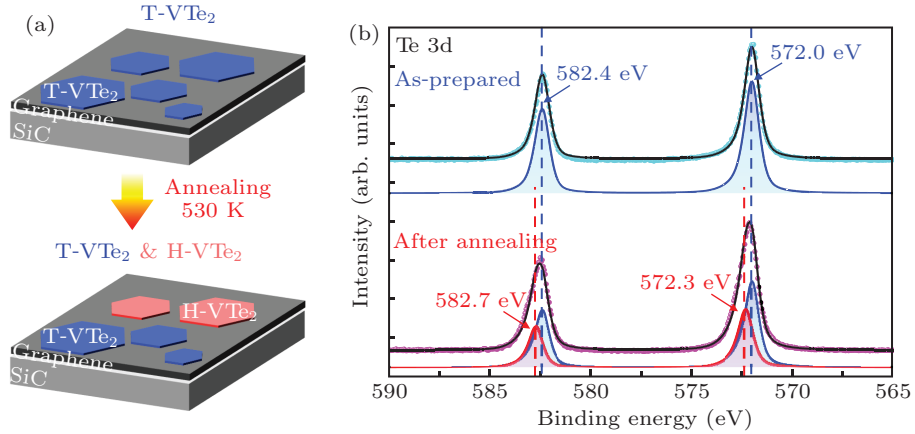


Fig. 1. XPS results of T-VTe_2 and T/H-VTe_2 samples. (a) Schematic diagram of the fabrication of the T/H-VTe_2 sample on the graphene substrate. (b) The Te 3d spectra of the T-VTe_2 (as-prepared) and T/H-VTe_2 sample (after annealing). The Te 3d peak positions (of pure T-VTe_2 at 582.4 eV and 572.0 eV, of T/H-VTe_2 mixture at 582.7 eV and 572.3 eV), showing an energy shift of 0.3 eV.

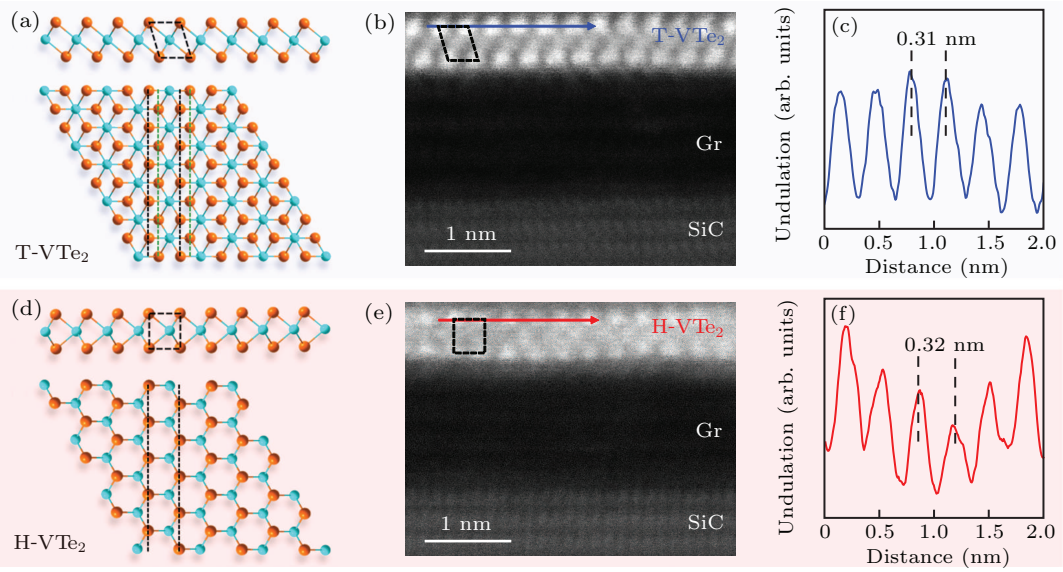


Fig. 2. The cross-section STEM results of T- and H-VTe_2. (a) and (d) The atomic models of T (a) and H-VTe_2 (d) in side view (upper) and top view (lower). (b) and (e) The cross-section HAADF-STEM images of T (b) and H-VTe_2 (e). The unit cells in side view are marked with black dashed frames. (c) and (f) The line profiles along the blue and red arrows in panels (b) and (e), respectively.

Moreover, atomic resolution STM measurements were carried out to reveal the CDW superlattice, to further characterize the atomic structure of the monolayer VTe_2. The zoom-in atomic resolution STM image, the corresponding line profile, and the fast Fourier transform (FFT) pattern of monolayer T-VTe_2, as shown in Figs. 4(a)–4(c), demonstrate the hexagonal atomic lattice with 0.35-nm lattice constant, without any superstructure. The angle-resolved photoemission spectroscopy (ARPES) results also reveal the electronic structure, which is the same as calculated (See Fig. S1 in Supplementary information) and previous reports.[25–27] These results agreed with its LEED pattern at RT in Fig. 3(c). As a comparison, the atomic resolution STM image of T-VTe_2 at 4.5 K is shown in Fig. 4(d), which clearly displays a superlattice, as the reported CDW pattern of T-VTe_2 below 186 K.[23,25–27] The line profile shown in Fig. 4(e) reveals the period of the CDW pattern is 1.42 nm. Combined with the 4×4 superlattice in the FFT pattern shown in Fig. 4(f), we can calculate the lattice constant of 0.35 nm, which agrees with the STM and STEM results mentioned above.

In contrast with the 4×4 CDW pattern of ML T-VTe_2 at 4.5 K, ML H-VTe_2 shows a $2\sqrt{3}\times 2\sqrt{3}$ CDW superlattice appearing at 300 K. From the atomic-resolution STM image shown in Fig. 5(a), we can see that the $2\sqrt{3}\times 2\sqrt{3}$ CDW superlattice clearly, as depicted. As shown in Fig. 5(b), the line profile indicates that the lattice constant of H-VTe_2 is 0.36 nm,

which is consistent with the STEM results. Moreover, the corresponding FFT pattern reveals the $2\sqrt{3} \times 2\sqrt{3}$ superlattice, which agrees with the same superlattice in LEED results. To investigate the strength of the CDW in H-VTe_2, we performed varied temperature LEED measurements at 400 K and 450 K, as shown in Figs. 5(d) and 5(e), respectively. From the LEED patterns, we can see the $2\sqrt{3} \times 2\sqrt{3}$ CDW superlattice of H-VTe_2 clearly, even at 450 K. Thus, the CDW transition temperature of H-VTe_2 is higher than 450 K, which means the CDW state is robust.

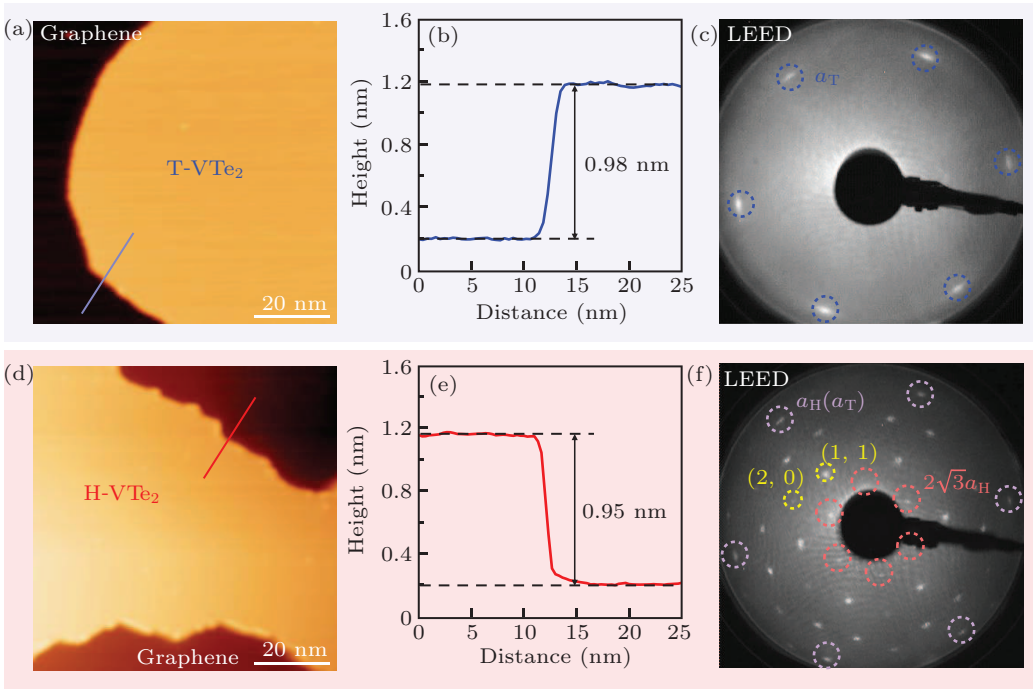


Fig. 3. Room-temperature STM and LEED results of the T-VTe_2 and T/H-VTe_2 samples. (a) and (d) STM topographic images (−2.0 V, 200 pA) of T-VTe_2 (a) and H-VTe_2 (d) islands, respectively. (b) and (e) Line profiles along the blue and red lines in panels (a) and (d), respectively. (c) and (f) LEED patterns of the T-VTe_2 and T/H-VTe_2 sample. The diffraction spots of T-VTe_2 (a_T), T/H-VTe_2 (a_H), H-VTe_2 superlattice ($2\sqrt{3}a_H$) and its secondary diffraction spots are marked with the blue, purple, red and yellow dotted circles, respectively.

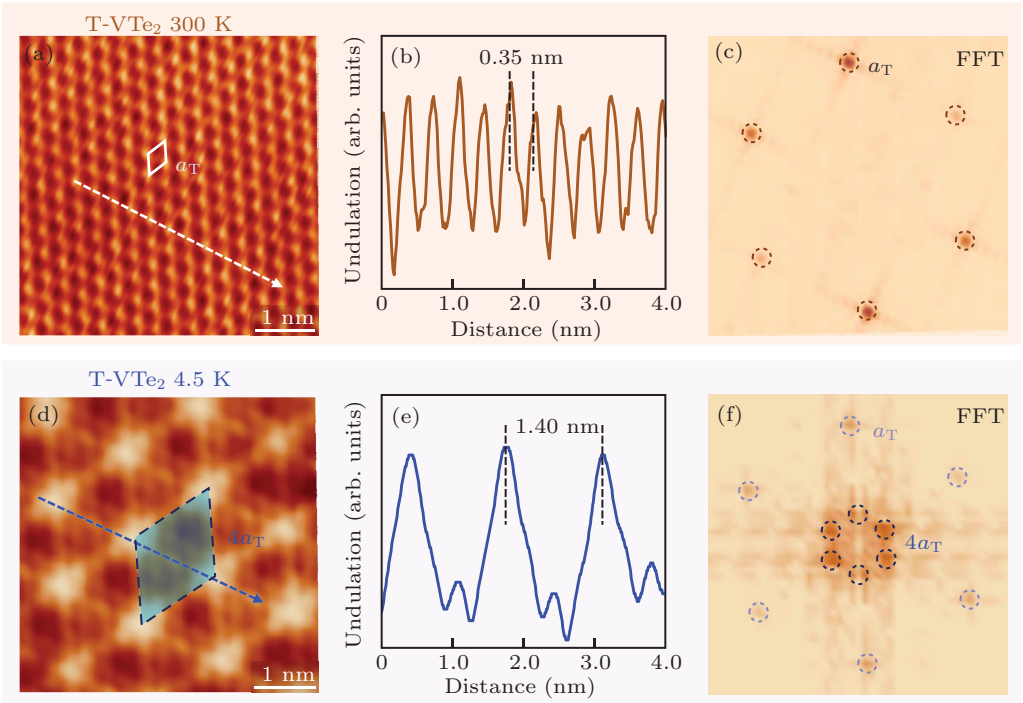


Fig. 4. Atomic-resolution STM images of T-VTe_2. (a) and (d) Atomic-resolution STM images of T-VTe_2 measured at 300 K (−0.1 V, 1 nA) (a) and 4.5 K (−50 mV, 1.5 nA) (d), respectively. The atomic lattice and CDW superlattice are depicted with white and blue dashed rhombus, respectively. (b) and (e) Line profiles along the white and blue dashed arrows in panels (a) and (d), respectively. (c) and (f) The FFT patterns of the STM images in panels (a) and (d), respectively. The spots of the atomic lattice at 300 K, 4.5 K, and the CDW superlattice are marked with black, purple, and blue dotted circles, respectively.

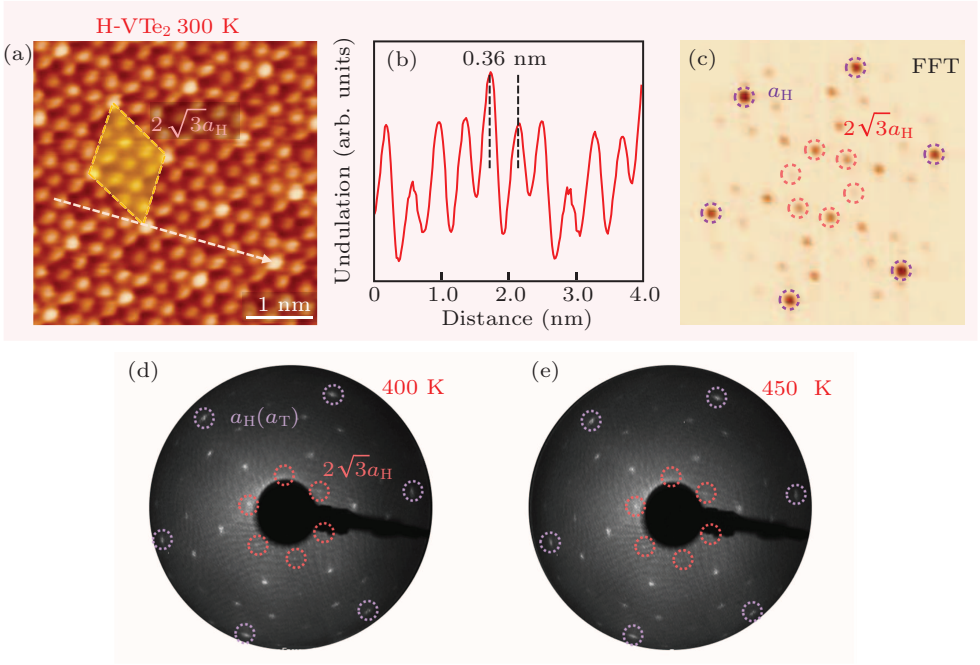


Fig. 5. CDW superlattice of H-VTe_2. (a) Atomic-resolution STM image (0.1 V, 2 nA) of H-VTe_2 measured at 300 K. The unit cell of CDW superlattice is depicted with the yellow dashed rhombus. (b) Line profile along the white dashed arrow in panel (a). (c) The FFT pattern of the image in panel (a). The spots of the H-VTe_2 atomic lattice and CDW superlattice are marked with purple and red dotted circles, respectively. (d) and (e) LEED patterns of the T/H-VTe_2 measured at 400 K and 450 K, respectively. The spots of the T/H-VTe_2 lattice and CDW superlattice are marked with purple and red dotted circles, respectively.

The Fermi-surface nesting[39] and the electron–phonon coupling[20,25] are the two common theories used to explain the origin of CDW in 2D TMDs. In the previous ARPES investigation of monolayer T-VTe_2, the CDW behavior in such a 2D layer was attributed to the Fermi-surface nesting of its anisotropic gaped Fermi contour.[25] While other observations by STM and STS mapping suggested that there could be other mechanisms contributing to VTe_2's CDW, which leads to the breaking of its three-folder symmetry. In the H-VTe_2 case, the CDW behavior becomes further complicated with the extreme robustness via temperature, which further indicates that mechanism other than Fermi-surface nesting and electron–phonon coupling is involved in the origin of its CDW. Moreover, in contrast with other TMDs, such as H-$TaSe_2$,[40] T-$TiSe_2$,[41] and T-VSe_2,[22] the higher CDW transition temperature of H-VTe_2 resembles those of the mott-insulating T-$NbSe_2$[42–44] and T-TaS_2,[4,45,46] in which the electron correlation take dominance. Whether some sort of electron correlation contributes to the origin of H-VTe_2's CDW still requires further investigation, but nevertheless, monolayer H-VTe_2 provides an ideal platform for exploring the mechanism behind the complicated CDWs in 2D-TMD systems.

3. Conclusion and perspectives

In summary, we report the 2D VTe_2 phase engineering and robust CDW state of monolayer H-VTe_2. Unlike the monolayer T-VTe_2 with a 4×4 CDW superlattice appearing only at low temperature, monolayer H-VTe_2 owns a $2\sqrt{3} \times 2\sqrt{3}$ CDW superlattice with a transition temperature above 450 K. Therefore, the 2D phase engineering offers an effective way for manipulating the CDW state of 2D TMDs. We believe the discovery of such an extremely robust CDW is useful for developing the applied 2D nanoelectronic devices based on the collective phenomenon.

Acknowledgements

Project supported by the National Key Research and Development Program of China (Grant Nos. 2021YFA1400100, 2020YFA0308800, and 2019YFA0308000), the National Natural Science Foundation of China (Grant Nos. 92163206, 62171035, 62171035, 61901038, 61971035, 61725107, and 61674171), the Beijing Nova Program from Beijing Municipal Science & Technology Commission (Grant No. Z211100002121072), and the Beijing Natural Science Foundation (Grant Nos. Z190006 and 4192054).

References

[1] Castro Neto A H 2001 *Phys. Rev. Lett.* **86** 4382
[2] Wen W, Dang C and Xie L 2019 *Chin. Phys. B* **28** 058504
[3] Si J G, Lu W J, Wu H Y, Lv H Y, Liang X, Li Q J and Sun Y P 2020 *Phys. Rev. B* **101** 235405
[4] Ishiguro Y, Bogdanov K, Kodama N, Ogiba M, Ohno T, Baranov A and Takai K 2020 *J. Phys. Chem. C* **124** 27176
[5] Wang R, Zhou J, Wang X, Xie L, Zhao J and Qiu X 2020 *Nano. Res.* **14** 1162
[6] Xie X, Lin D, Zhu L, Li Q, Zong J, Chen W, Meng Q, Tian Q, Li S C, Xi X, Wang C and Zhang Y 2021 *Chin. Phys. Lett.* **38** 107101
[7] Dang C, Guan M, Hussain S, Wen W, Zhu Y, Jiao L, Meng S and Xie L 2020 *Nano Lett.* **20** 6725

[8] Wang X, Liu H, Wu J, Lin J, He W, Wang H, Shi X, Suenaga K and Xie L 2018 *Adv. Mater.* **30** 1800074

[9] Liu G, Debnath B, Pope T R, Salguero T T, Lake R K and Balandin A A 2016 *Nat. Nanotechnol.* **11** 845

[10] Patel T, Okamoto J, Dekker T, Yang B, Gao J, Luo X, Lu W, Sun Y and Tsen A W 2020 *Nano Lett.* **20** 7200

[11] Liu H, Wu T, Yan X, Wu J, Wang N, Du Z, Yang H, Chen B, Zhang Z, Liu F, Wu W, Guo J and Wang H 2021 *Nano Lett.* **21** 3465

[12] Wang J, Guo C, Guo W, Wang L, Shi W and Chen X 2019 *Chin. Phys. B* **28** 046802

[13] Manzeli S, Ovchinnikov D, Pasquier D, Yazyev O V and Kis A 2017 *Nat. Rev. Mater.* **2** 17033

[14] Yang H, Kim S W, Chhowalla M and Lee Y H 2017 *Nat. Phys.* **13** 931

[15] Voiry D, Mohite A and Chhowalla M 2015 *Chem. Soc. Rev.* **44** 2702

[16] Wilson J A, Di Salvo F J and Mahajan S 1975 *Adv. Phys.* **24** 117

[17] Yoo Y, DeGregorio Z P, Su Y, Koester S J and Johns J E 2017 *Adv. Mater.* **29** 1605461

[18] Qu Y, Medina H, Wang S W, Wang Y C, Chen C W, Su T Y, Manikandan A, Wang K, Shih Y C, Chang J W, Kuo H C, Lee C Y, Lu S Y, Shen G, Wang Z M and Chueh Y L 2016 *Adv. Mater.* **28** 9831

[19] Su J, Wang M, Li Y, Wang F, Chen Q, Luo P, Han J, Wang S, Li H and Zhai T 2020 *Adv. Funct. Mater.* **30** 2000240

[20] Zhang D, Ha J, Baek H, Chan Y H, Natterer F D, Myers A F, Schumacher J D, Cullen W G, Davydov A V, Kuk Y, Chou M Y, Zhitenev N B and Stroscio J A 2017 *Phys. Rev. Mater.* **1** 024005

[21] Liu Z L, Wu X, Shao Y, Qi J, Cao Y, Huang L, Liu C, Wang J O, Zheng Q, Zhu Z L, Ibrahim K, Wang Y L and Gao H J 2018 *Sci. Bull.* **63** 419

[22] Chen P, Pai W W, Chan Y H, Madhavan V, Chou M Y, Mo S K, Fedorov A V and Chiang T C 2018 *Phys. Rev. Lett.* **121** 196402

[23] Miao G, Xue S, Li B, Lin Z, Liu B, Zhu X, Wang W and Guo J 2020 *Phys. Rev. B* **101** 035407

[24] Liu M Z, Wu C W, Liu Z Z, Wang Z Q, Yao D X and Zhong D 2020 *Nano. Res.* **13** 1733

[25] Wang Y, Ren J, Li J, Peng H, Yu P, Duan W and Zhou S 2019 *Phys. Rev. B* **100** 241404

[26] Coelho P M, Lasek K, Nguyen Cong K, Li J, Niu W, Liu W, Oleynik, II and Batzill M 2019 *J. Phys. Chem. Lett.* **10** 4987

[27] Wong P K J, Zhang W, Zhou J, Bussolotti F, Yin X, Zhang L, N'Diaye A T, Morton S A, Chen W, Goh J, de Jong M P, Feng Y P and Wee A T S 2019 *ACS Nano* **13** 12894

[28] Chen W, Zhang J M, Nie Y Z, Xia Q L and Guo G H 2020 *J. Magn. Magn. Mater.* **508** 166878

[29] Wasey A H M A, Chakrabarty S and Das G P 2015 *J. Appl. Phys.* **117** 064313

[30] Li F, Tu K and Chen Z 2014 *J. Phys. Chem. C* **118** 21264

[31] Kan M, Wang B, Lee Y H and Sun Q 2014 *Nano. Res.* **8** 1348

[32] Liu J, Hou W J, Cheng C, Fu H X, Sun J T and Meng S 2017 *J. Phys.: Condens Matter* **29** 255501

[33] Manchanda P and Skomski R 2016 *J. Phys.: Condens Matter* **28** 064002

[34] Rasmussen F A and Thygesen K S 2015 *J. Phys. Chem. C* **119** 13169

[35] Ji S, Wu H, Zhou S, Niu W, Wei L, Li X A, Li F and Pu Y 2020 *Chin. Phys. Lett.* **37** 087505

[36] Kresse G and Furthmuller J 1996 *Phys. Rev. B* **54** 11169

[37] Blochl P E 1994 *Phys. Rev. B* **50** 17953

[38] Perdew J P, Burke K and Ernzerhof M 1996 *Phys. Rev. Lett.* **77** 3865

[39] Borisenko S V, Kordyuk A A, Zabolotnyy V B, Inosov D S, Evtushinsky D, Buchner B, Yaresko A N, Varykhalov A, Follath R, Eberhardt W, Patthey L and Berger H 2009 *Phys. Rev. Lett.* **102** 166402

[40] Ryu H, Chen Y, Kim H, Tsai H Z, Tang S, Jiang J, Liou F, Kahn S, Jia C, Omrani A A, Shim J H, Hussain Z, Shen Z X, Kim K, Min B I, Hwang C, Crommie M F and Mo S K 2018 *Nano Lett.* **18** 689

[41] Chen P, Chan Y H, Fang X Y, Mo S K, Hussain Z, Fedorov A V, Chou M Y and Chiang T C 2016 *Sci. Rep.* **6** 37910

[42] Liu L, Yang H, Huang Y, Song X, Zhang Q, Huang Z, Hou Y, Chen Y, Xu Z, Zhang T, Wu X, Sun J, Huang Y, Zheng F, Li X, Yao Y, Gao H J and Wang Y 2021 *Nat. Commun.* **12** 1978

[43] Nakata Y, Sugawara K, Shimizu R, Okada Y, Han P, Hitosugi T, Ueno K, Sato T and Takahashi T 2016 *NPG. Asia. Mater.* **8** e321

[44] Nakata Y, Sugawara K, Chainani A, Oka H, Bao C, Zhou S, Chuang P Y, Cheng C M, Kawakami T, Saruta Y, Fukumura T, Zhou S, Takahashi T and Sato T 2021 *Nat. Commun.* **12** 5873

[45] Sipos B, Kusmartseva A F, Akrap A, Berger H, Forro L and Tutis E 2008 *Nat. Mater.* **7** 960

[46] Hu Q, Yin C, Zhang L, Lei L, Wang Z, Chen Z, Tang J and Ang R 2018 *Chin. Phys. B* **27** 017104